ACS OMEGA

Open Access

http://pubs.acs.org/journal/acsodf

Article

Design and Synthesis of Ketenimine Sulfonamide Conjugates through Multicomponent Reactions; A Combined Cytotoxic Analysis and Computational Exploration

Deepak J. Prabhu, Ujjayinee Ray, Anjaly Rajeev, Reshma Joy, Abi Thoppilan George, Jinu George, Sathees C. Raghavan, and Franklin John*

Cite This: *ACS Omega* 2023, 8, 38619−38631

Read Online

ACCESS | Metrics & More | Article Recommendations | Supporting Information

ABSTRACT: Multicomponent reactions involving zwitterion generated from dimethyl acetylenedicarboxylate, aryl sulfonamide, and isocyanide to generate sulfonamide-conjugated ketenimines is reported. The synthetic strategy adopted is highly atom economical and stereoselective. Ketenimine sulfonamide analogues are key intermediates for further synthetic conversions to generate a combinatorial library of compounds. Furthermore, sulfonamide compounds are known to possess a broad spectrum of biological applications. All the novel molecules synthesized exhibit the potential to target the nonhomologous DNA end-joining (NHEJ) pathway with cytotoxic ability. Computational studies compliment the in vitro biological assays of the 8 small-molecule inhibitors. DNA double-strand breaks (DSBs) are considered as the most lethal among different DNA damages. NHEJ repairs about 70% of the DSBs generated in cells within mammals. The DNA-dependent protein kinase catalytic subunit is one of the PI3 kinases associated with NHEJ. Compounds DK01−DK08 were investigated for their ability to induce cancer cell death by treating with two leukemic cell lines where NHEJ is high. Results showed that bromoaryl (DK04)- and nitroaryl (DK05)-conjugated molecules showed excellent biological activity, having IC_{50} values of ∼2 μM in Nalm6 cell lines.

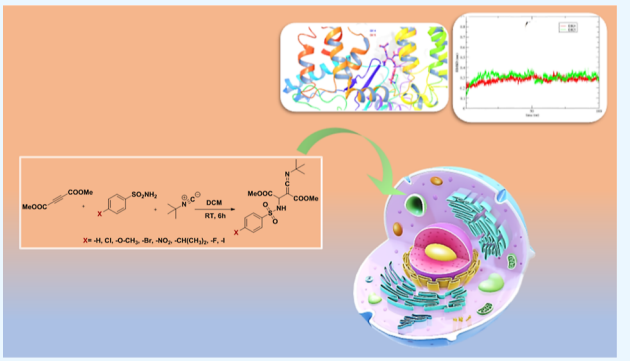

1. INTRODUCTION

Cancer remains as a global health concern and a leading cause of death worldwide.[1] Even though there is significant improvement in medicinal chemistry research recently leading to treatment options for cancer, especially when it is in the early stage, the mortality rate is still high across the globe.[2,3] The number of mortalities due to leukemia, colon, and liver cancer is increasing rapidly. Synthetic development of potential anticancer agents having low side effects is highly desirable to combat this deadly disease. A large number of mutagenic processes allow cancer cells to acquire properties of unlimited proliferation potential, self-sufficiency in growth signals, and resistance to both antiproliferative and apoptotic cues which would, otherwise, contain their growth.[4−8]

Maintenance of genomic integrity is critical for the existence of any organism.[9−17] DNA in our cells encounters thousands of lesions on a daily basis. Among DNA damages, double-strand breaks (DSBs) are one of the most harmful lesions to a cell.[18,19] Failure in DSB repair could lead to genomic instability and cancer.[20−22] Nonhomologous DNA end joining (NHEJ) is the major DNA double strand repair pathway in mammals.[19,23] Cancer cells differ in the efficiency of NHEJ.[21,24] Major proteins involved in NHEJ are the Ku70/80 heterodimer, the DNA-dependent protein kinase catalytic subunit (DNA-PKcs), Artemis, and the NHEJ ligase complex (LigIV/XRCC4/XLF).[25,26] DNA-PK is a 460 kDa kinase and the kinase activity is essential for NHEJ. Tyrosine kinase is another family member of kinases, which helps to send growth signals in cells, and blocking them stops the cell growth and division.[27] Inhibitors of tyrosine kinases are potential anticancer agents.[22]

Specific targeting of NHEJ machinery by novel synthetic molecules offers a strategy for the development of cancer therapeutics.[24,28] Among the NHEJ inhibitors, metabolite Wortmannin and KU-0060648 are dual inhibitors of DNA-PK and phosphatidyl inositol 3-kinase (PI3K).[21] NU7441 (or KU57788) and M3814 are selective inhibitors for DNA-PK, currently undergoing clinical trial for cancer.[29] Novel synthetic agents targeting the NHEJ pathway are in high demand in therapeutic development.

Received: August 8, 2023
Accepted: September 25, 2023
Published: October 5, 2023

Heterocyclic systems with cytotoxic potential are recently reported.[4] Ketenimines are known as synthetic intermediates targeting the core of potent topoisomerase inhibitor Tas-103.[30] Interestingly, there are no reports of ketenimines targeting DNA-PK or other proteins in the NHEJ pathway. The synthetic applications of ketenimines are comparable to that of the isoelectronic species ketenes and allenes.[31,32] A variety of procedures including couplings, eliminations, rearrangements, and click chemistry are known till date for ketenimine synthesis.[33−36]

Herein, we report the design and synthesis of ketenimines by multicomponent reactions (MCRs). MCRs offer a green chemistry approach with regard to the atom economy. MCRs are popular due to their simple procedure, high atom economy, and wide variety of products.[37−39] In one pot synthesis, reactants for two or three steps are mixed initially, and under a given set of conditions, the reactions occur in sequential order to give a diverse variety of products that incorporates all the reactants. These reactions will produce very little waste and hence are eco-friendly and reduce the time/cost of synthesizing bioactive drugs.[40,41] Isocyanide-based MCRs pass through the formation of zwitterionic intermediate and give chiral products, which possess the features of naturally occurring drugs and are successfully used as drugs for targeting many proteins.[40−43] The power of MCRs was revealed by the discovery of a low-molecular-weight CCR5 antagonist, which can be used as a drug target to treat HIV infections.[44] The biocompatibility and specificity of biomolecules such as peptides, proteins, and antibodies make these macromolecules ideal carriers for selective targeted therapies. A novel cytotoxic anti-HER2 antibody drug conjugate was reported by Albericio et al. through Ugi-MCR, elaborating the synthetic use of these type of reactions.[45]

Sulfonamides constitute an important class of drugs, with many types of pharmacological agents possessing antibacterial, anticarbonic anhydrase, antiobesity, diuretic, hypoglycemic, antithyroid, antitumor, and antineuropathic pain activities.[46−48] Ketenimine derivatives from 2-pyridinone and 4-quinazolinone have considerable antibacterial activity against *Staphylococcus aureus* and *Escherichia coli* standard strains. Trimethylated ketenimines and 1-aza butadienes derived from 4-quinazolinone showed acceptable antifungal activity against *Candida albicans*.[49] Ketenimines can potentially be synthesized by MCRs by a variety of procedures.[50−52] They consist of sulfonamide and amide functional groups, which form a part of natural products and drugs possessing a wide spectrum of inevitable bioactivity in medicinal chemistry.[53] Ketenimines derived from aromatic sulfonamide that contain both sulfonamide and ketenimine scaffolds are expected to show high bioactivity and can be used to target enzymes. Notably, Chur Chin et al. synthesized a sulfonamide derivative that specifically inhibits protein kinase A, a central factor in the NHEJ process. Additionally, this compound has proven to suppress stress-responsive genes, including DNA-PKcs (DNA-PK catalytic subunit).[54] A class of compounds belonging to the ketenimine family are known to be potent pharmacology relevant molecules.[55] Thus, we have attempted the synthesis of ketenimine sulfonamides by efficient three-component reactions to identify potential anticancer agents.

We have synthesized a series of 8 compounds (DK01 to DK08), and cytotoxic investigations were done. After identifying the cytotoxic potential of the novel molecules, we have done computational investigations based on molecular docking using the popular autodock tool to check the potency of the ketenimines as inhibitors of all known target proteins in the NHEJ pathway. As per the protein−ligand docking algorithm of autodock, the higher negative value of docking scores of ligands (DK compounds in the present case) to the target proteins is an indication of strong binding affinity. Docking scores of all DK compounds (Supporting Information) to all target proteins in the NHEJ pathway range from −6.0 to −7.4 kcal/mol except in the case of the DNA-dependent protein kinase (DNA-PK). However, the docking scores of all DK compounds to the DNA-PK target range from −8 to −9 kcal/mol. These results point out the significant binding of DK compounds to the active site of the DNA-PK (PDB ID: 5Y3R Chain C-Catalytic residues 3676−4100), which potentially can act as the most probable target in the NHEJ pathway.[17,56] Further, we performed the protein−ligand molecular dynamics simulation investigations followed by molecular mechanics Poisson−Boltzmann surface area (MM-PBSA) binding energy calculations to confirm the inhibitory activity of these compounds against protein kinase subunit. The docking scores and MM-PBSA binding energies confirmed the inhibitory activity of all compounds against the protein kinase subunit, which is presumed to be a prominent target in the NHEJ pathway. Thus, our investigations have shown the effects of ketenimines for the first time on DNA-PK.

2. RESULTS

The smooth 1:1:1 three-component reaction was carried out to produce selectively stable ketenimine sulfonamides (DK01−DK08) in dichloromethane at room temperature to yield crystalline products. Isocyanides, dialkyl acetylene dicarboxylates, and sulfonamides were used as building blocks. A published procedure was adopted for the synthesis of all novel compounds (DK01−DK08).[55]

All compounds in the DK series possess only one stereogenic center (Figure 1a) and thus, one pair of enantiomers are expected. The single-crystal X-ray analysis of the previously reported analogous compound (Figure 1b) suggested that the reaction yields only one form, which is the "S" configurational isomer.[55] HPLC chromatograms of all the crystalline compounds indicated the presence of a single isomer (Supporting Information). A representative HPLC profile is shown in Figure 2.

We were interested in investigating whether small molecules were involved in inducing cell death in cancer cell lines. Human B cell leukemic cell line, Nalm6, and human T cell leukemic cell line, CEM cell lines were used to evaluate the cytotoxic potential of DK01−DK08. Expression of NHEJ proteins including DNA-PK and the efficiency of end joining in vitro are reportedly moderate to good in these cell lines.[28,57,58] Interestingly, after 48 h of incubation with the compounds, several of them showed a cytotoxic effect in cancer cell lines. In Nalm6, DK01−DK05 showed increased cell death at concentrations as low as 2 μM (Figure 3). Particularly at high concentrations of 50 and 100 μM, very few viable cells or no viable cells were observed in these cases (Figure 3). In the case of DK06, DK07 and DK08, viable cells were observed even at the highest concentration of 100 μM, suggesting the less cytotoxic potential of these compounds (Figure 3). IC_{50} values were calculated with respect to % of viable cells and concentrations of the compounds. Interestingly, the lowest IC_{50} was obtained for DK05 at 2.57 μM, followed by DK04 at

https://doi.org/10.1021/acsomega.3c05816
ACS Omega 2023, 8, 38619−38631

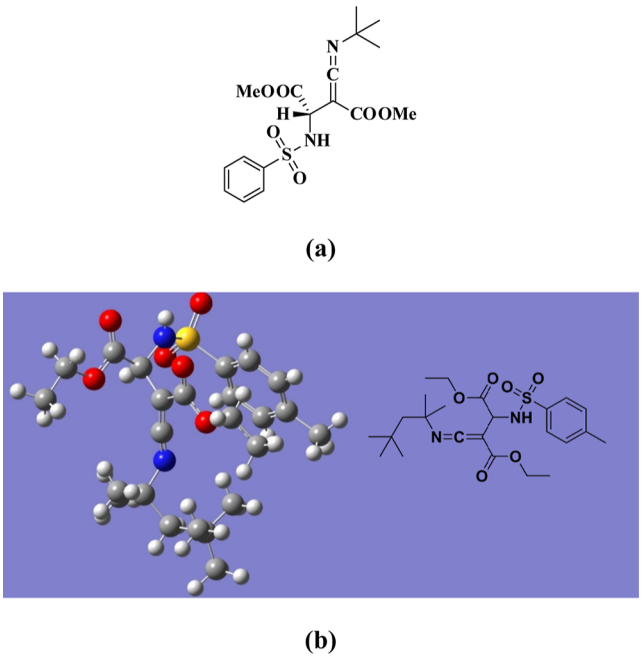

Figure 1. (a) Optimized structure of DK01. (b) Structure (generated using Gauss view software) of the ketenimine sulfonamide derivatives synthesized by Shaabani et al.[55] The structure is from ref 55 and is reproduced after copyright permission from the Royal Society of Chemistry [2011].

2.80 μM (Table 1). DK02exhibited IC_{50} of 8 μM, while DK01 and DK03 showed a similar 11 μM IC_{50} value (Table 1). IC_{50} of DK07 and DK08 were >80 μM (Table 1), which is quite high for any compound showing an anticancer effect. Thus, among all of the compounds of the series, DK04 and DK05 showed the best cytotoxicity with the lowest IC_{50} of ~2 μM in Nalm6.

Cytotoxicity was also checked for the compounds in CEM cell line. Cells were similarly treated with increasing concentrations of the compounds (1, 2, 5, 10, 50, 100 μM) for 48 h. Very few viable cells (<20%) were obtained at the highest concentration of 100 μM for DK02, DK05, DK06, and DK07 (Figure 4). CEM cells were not sensitive to the other compounds at 50 and 100 μM concentrations, suggesting a low cytotoxic potential of these compounds (Figure 4). The cells were the least sensitive to DK01 treatment. Determination of IC_{50} values revealed that DK06 was the most cytotoxic, with IC_{50} 23.43 μM (Table 2). DK01 and DK07 were the least cytotoxic among the compounds, with IC_{50} > 90 μM (Table 2). IC_{50} values for other compounds were between 20 and 50 μM. Thus, in CEM, DK06 showed better cytotoxicity than all other compounds.

We have evaluated the cytotoxic potential of DK series (DK01−DK08) compounds in two leukemic cancer cell lines, Nalm6 and CEM. In Nalm6, DK04 and DK05 showed the lowest IC_{50}, while in CEM, DK05 and DK06 showed a better effect among all other compounds in the series. However, in CEM, IC_{50} for DK04 was ~41 μM, which is toward the higher side in terms of induction of cancer cell death and a possible therapeutic application. Interestingly, DK05 showed IC_{50} ~ 2 μM in Nalm6, which is the lowest among the compounds tested. Taking the results from two cell lines into account, DK05 showed a better cytotoxicity in both cells and, therefore, can be harnessed for future experiments.

2.1. Molecular Docking Studies. The binding affinity of all DK compounds at the active site of a kinase target was quantitatively examined using the molecular docking calculations. All DK series compounds possess docking scores between −8 and −9 kcal/mol, indicating their putative inhibitory activity against the kinase target. The best docking poses of DK01−DK03 and DK04−DK05 are pictorially represented in Figure 5a,b, respectively. The docking scores corresponding to the best docking poses for ligands from DK01 −08 are −8.5, −8.5, −8.7, −8.8, −8.8, −8.4, −8.4, and −8.2 kcal/mol, respectively. The higher negative docking scores of all DK series compounds near the active site of kinase target were due to the presence of strong protein−ligand nonbonding interactions such as hydrogen bonding and hydrophobic interactions. It is well-known that such interactions play a key role in stabilizing a small molecule energetically in the binding pocket of a protein. Commonly, six amino acid residues of the kinase target strongly interact with all DK compounds through hydrogen bonds and hydrophobic contacts. The 3D representation of best docking pose of DK01−kinase complex with protein−ligand interactions is shown in Figure 6 as this is a common case. The residues Arg3612 and Arg3799 exhibit hydrogen bonding interactions with the carboxylate oxygen atoms of DK compounds. Lys3608 and Phe3542 show alkyl−alkyl (hydrophobic) interactions with the trimethyl groups of the DK series. Ala3616 and Leu3584 residues are connected with the aryl

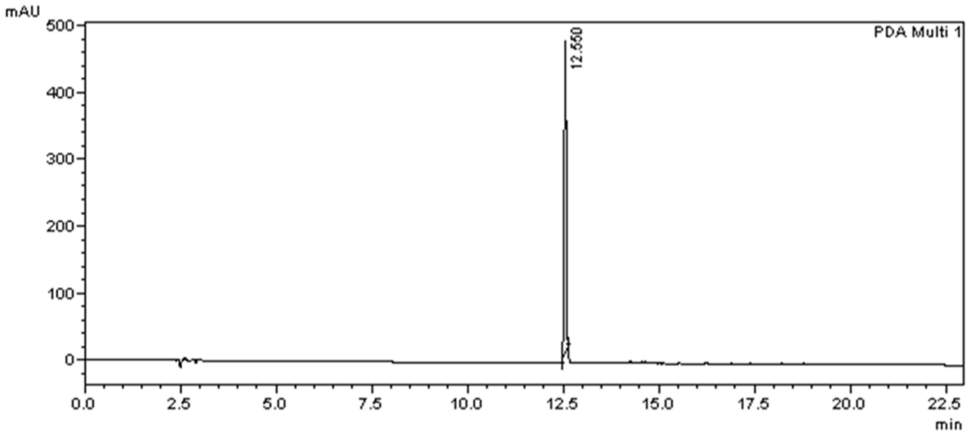

Figure 2. HPLC profile of DK03.

https://doi.org/10.1021/acsomega.3c05816
ACS Omega 2023, 8, 38619−38631

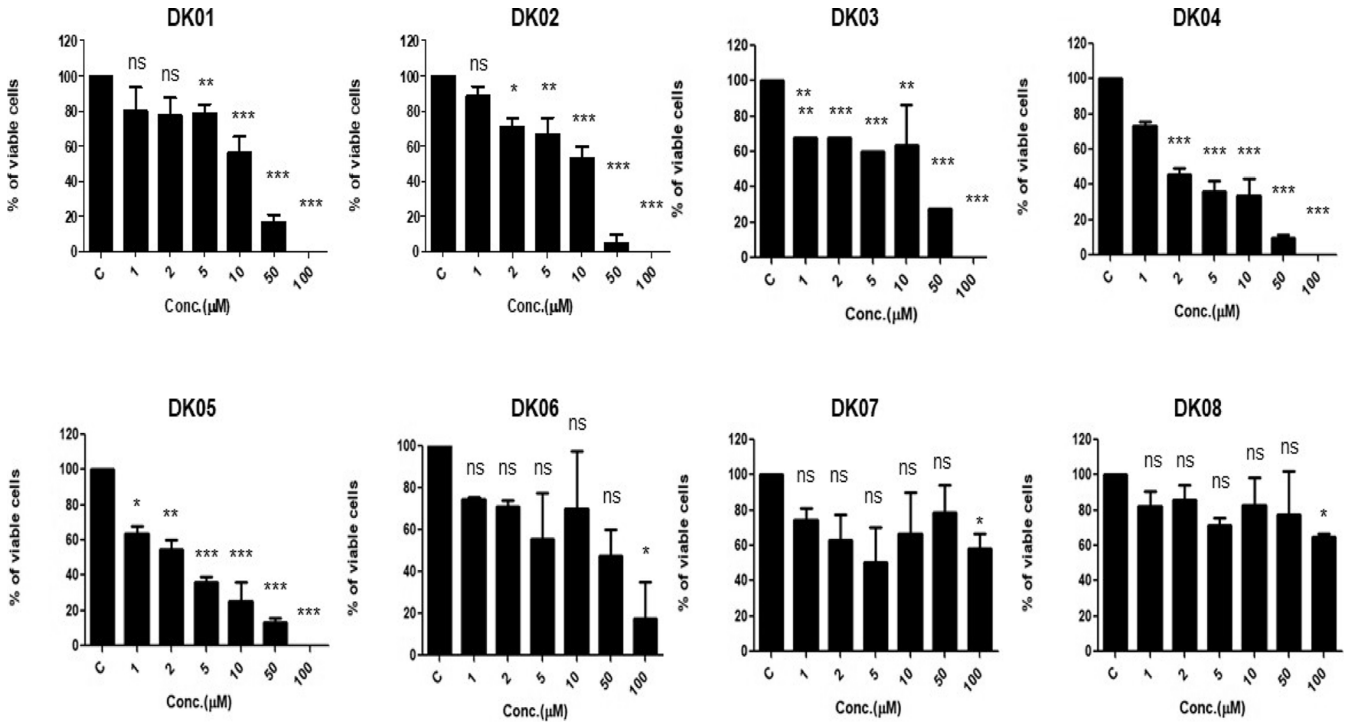

Figure 3. Bar diagram showing cytotoxicity of DK series in the Nalm6 cell line. Cells were treated with increasing concentrations of the compounds (1, 2, 5, 10, 50, and 100 μM) for 48 h. Control cells were treated with equivalent DMSO. Bar graphs for Nalm6 were plotted using % of viable cells and concentration of compounds.

Table 1. IC_{50} Values of DK01−DK08 in the Nalm6 Cell Line at 48 h

DK series	IC_{50} (μM)
DK01	11.04
DK02	8.11
DK03	11.27
DK04	2.80
DK05	2.57
DK06	17.84
DK07	86.20
DK08	143.95

group of ligands through π-alkyl (hydrophobic) interactions. A few additional nonbonding interactions were also present in the docking pose of each DK compound due to the difference in its alkyl group. The 2D representation of protein ligand interactions of best docking poses of all DK series is provided in the Supporting Information.

In conclusion, all DK compounds under investigation have been found to fit well into the binding site of the kinase target. Based on the docking scores, the order of binding affinity of all DK compounds to the target with slight differences is given as DK04 = DK05 > DK03 > DK01 = DK02 > DK06 = DK07 > DK08. This is consistent with the IC_{50} values of the compounds in the cancer cell lines (Table 3). Apart from this, DK06 and DK02 also showed better IC_{50} in CEM among all of the compounds tested, which requires further investigation. Further the protein−ligand complex structures with best docking poses have been chosen for molecular dynamics simulations. More specific and quantitative results of DK compounds and their activity against kinase target were obtained from the simulation studies followed by MM-PBSA calculations.

2.2. MD Trajectory Analysis and MM-PBSA Binding Energy Calculations. This section discusses the findings from post-MD analysis of the kinase−DK complex systems. As the protein−ligand binding energies and subsequent MD results of DK01−DK05 complexes show close correlation with the experimental IC_{50} data, we have included the same in this analysis session. The equilibration and stability of all simulated systems are evaluated in terms of the root-mean-square deviation (RMSD) of the complex system from the starting conformation and the root-mean-square fluctuation (RMSF) of protein residues in the MD trajectory.

The RMSD of all of the protein−ligand complexes lies within 0.30 nm from their starting conformations over the course of the simulation. However, the DK03 (Figure 7a) complex shows fluctuations above 0.4 nm at the beginning, which stabilized to 0.3 nm deviations during the course of time. The steady RMSD plots (Figure 7a,b) with minimal changes in the same 100 ns MD trajectory is a sign of stable protein−ligand complex formation in solvated systems. Further, we have evaluated the protein residue's contribution to the conformational alterations of every complex in the MD trajectory (Figure 8) as RMSFs. The average fluctuation of the ligand binding site residues is 0.2−0.3 nm. With the exception of a few terminal residues, almost all binding site residues of the target (Figure 8a,b) exhibit strong levels of conservation during the MD production run, with a minimum fluctuation of 0.2 nm. Again, a few more protein residues of the DK03 complex show fluctuations above 0.5 nm. Even in this case, the binding site residues from 3542 to 3800 with less fluctuations will not disturb the total stability of the DK03 complex system.

2.3. MM-PBSA Binding Energies. Here, we report the results of MM-PBSA calculations obtained by utilizing 1500 snapshots taken at 20 ps intervals between 71 and 100 ns from the MD trajectory. The MM-PBSA protein ligand binding

https://doi.org/10.1021/acsomega.3c05816
ACS Omega 2023, 8, 38619−38631

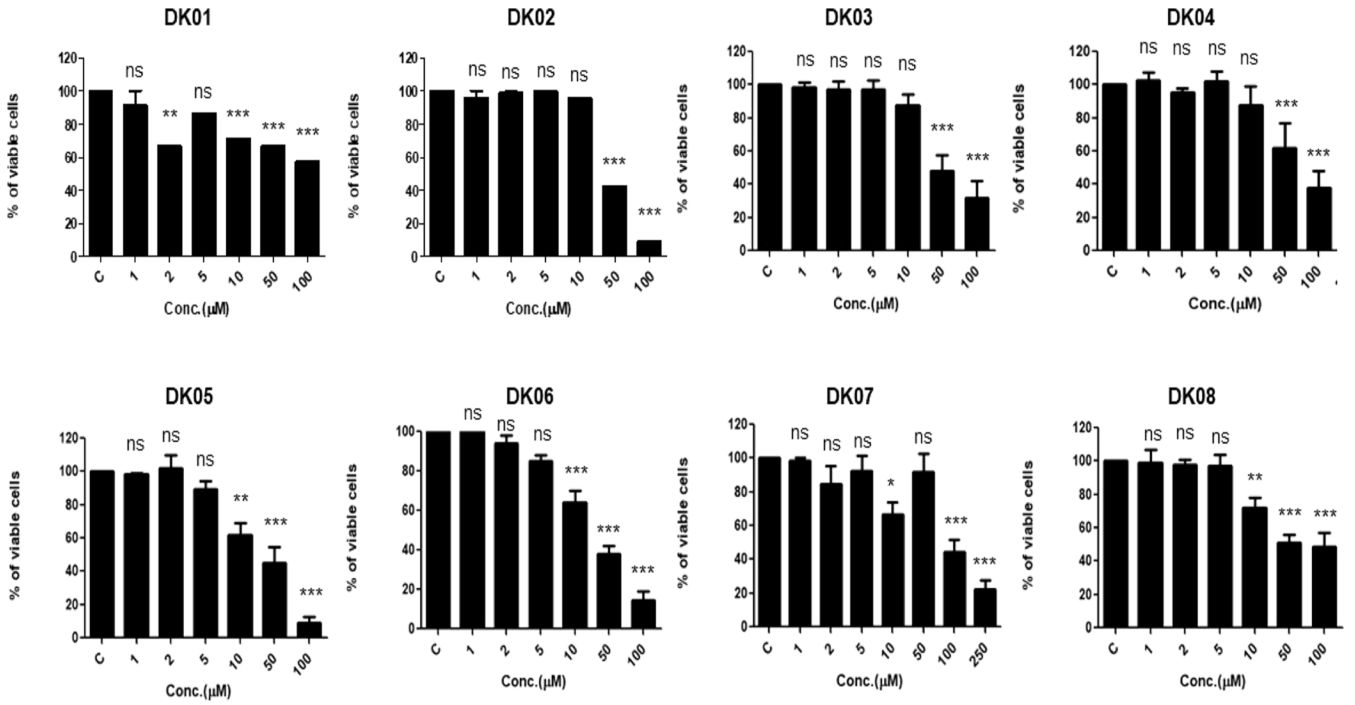

Figure 4. Bar diagram showing cytotoxicity of DK series in CEM cell line. Cells were treated with increasing concentrations of the compounds (1, 2, 5, 10, 50, and 100 μM) for 48 h. Control cells were treated with equivalent DMSO. Bar graphs for CEM were plotted using % of viable cells and concentration of compounds.

Table 2. IC_{50} Values of DK01−DK08 in the CEM Cell Line at 48 h

DK series	IC_{50} (μM)
DK01	92.63
DK02	38.16
DK03	50.71
DK04	41.76
DK05	24.43
DK06	23.43
DK07	94.83
DK08	50.60

energies with minimum standard deviation (10 kJ/mol<) and its subcomponents shown in Table 4 are further validated using 10 ns MD replicates. The higher negative van der Waal energy obtained as a result of strong protein−ligand hydrophobic interactions is primarily responsible for the bigger $-\Delta G$ value and strong binding affinity. Additionally, the MM-PBSA binding energy is also influenced by the electrostatic energy (mainly through protein−ligand hydrogen bonds) and the solvent accessible surface area energy, both of which have negative values. However, the overall negative value of the binding energy is decreased by the rise in the polar solvation energy with positive energy values. As per the MM-PBSA binding energy estimates, the order of binding affinity of DK series of compounds against a target kinase is interpreted as DK04 > DK05 > DK03 > DK01 > DK02 > DK06 > DK07 > DK08 (Table 4). Thus, DK04 and DK05 compounds are considered as best inhibitors of a protein kinase in these results. Using the code "energy2bfac" implemented in g_mmpbsa, we have deduced the energy contribution of individual protein−ligand residues to the total binding energy via subcomponents.

The energy contributions of ligand residues DK01−DK05 to the MM-PBSA binding energy were found to be −62.90, −61.09, −63.0, −69.29, and −67.95 kJ/mol, respectively. The larger negative values of energy contribution of DK04 and DK05 are an indication of its high binding affinity to the kinase target. The data of protein residues (hot spot residues) in complexation with DK01, which possess large negative energies as MM-PBSA binding energies, are shown in Figure 9a. The details of protein residues (bad contact residues) with positive energy value contributions to MM-PBSA energy were also included in the same plot. Subsequently, the detailed nonbonding interaction profile (generated using LIGPLOT) obtained from the protein−ligand conformation of DK01 used in MM-PBSA calculations are given in Figure 9b. Further, the MM-PBSA energies of (hot spot and bad contact) protein residues in DK02, DK03, DK04, and DK05 complexes are presented in Figure 10a,b and 11a,b, respectively. Similar to the nonbonding interaction profile of the DK01−kinase complex in Figure 9b, the same profiles for DK02, DK03, DK04, and DK05 complexes are shown in Figure 12a,b and 13a,c, respectively.

The hot spot residues with high negative energy contribution in the DK01 complex (Figure 9a) are Ala3616 (−8.16), Arg3799 (−6.97), Met3609 (−4.88), and Arg3612 (−4.71) respectively. All of these hot spot residues except Arg3799 had hydrophobic contacts (Figure 9b) with the DK01 compound in the MD trajectory. As expected, the binding of DK01 complex is facilitated with hydrophobic interactions rather than the hydrogen-bonded residue Arg3799.

Analysis of the DK04 complex having higher binding affinity revealed that the significant hot spot residues with high negative energy contribution (Figure 11a) are Leu3584 (−7.82), Ala3612 (−5.97) Asp3591 (−5.46), and Ala3616 (−4.39), respectively. Except Arg3612, all other residues showed strong hydrophobic interactions with DK04 as

https://doi.org/10.1021/acsomega.3c05816
ACS Omega 2023, 8, 38619−38631

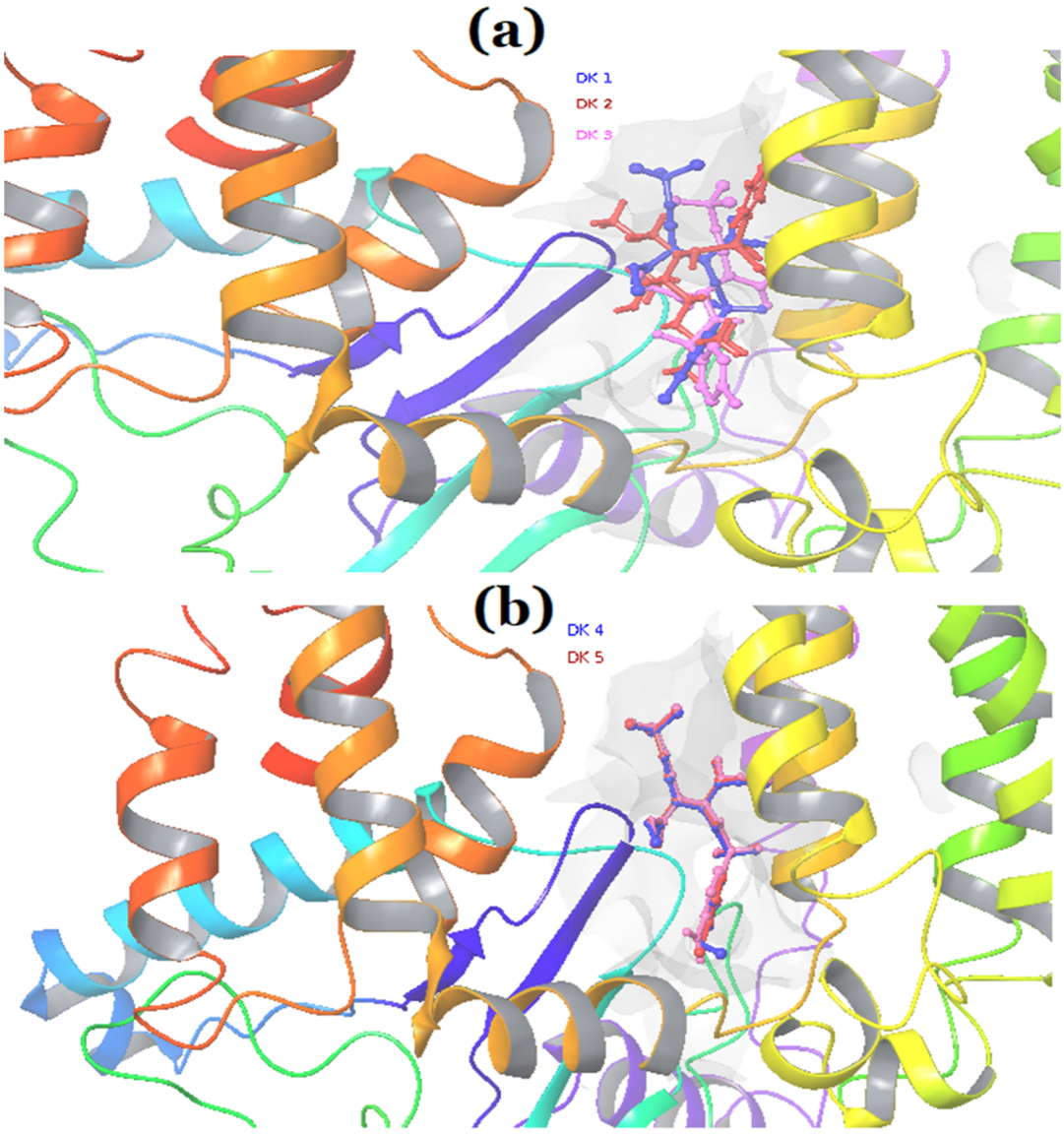

Figure 5. Aligned docking poses of (a) DK01, DK02, DK03, and (b) DK04, DK05 compounds, respectively, in the active site of the protein kinase. Protein residues and DK ligands are shown by ribbon and ball/stick representations, respectively. The specific DK compound can be identified from its colored labels.

illustrated in Figure 13a. Meanwhile, Arg3612 is found to be involved in hydrogen bonding interactions. Leu3584 and Thr3797 with energy contributions −10.89 and −6.2 kJ/mol, respectively, exhibit strong hydrophobic interactions with DK05 (Figures 11b and 13b), which is considered as the next best binder to the kinase protein. The Leu3584 residue also exhibited consistent hydrophobic interactions with DK02 and DK03 complexes with energy contributions of −7.52 and −9.99 kJ/mol, respectively. The Leu3800 residue showed the same trend in DK02 (−5.21 kJ/mol) and DK03 (−8.59 kJ/mol) complexes with negative free energy contributions to the MM-PBSA binding energies. Leu residues (3584 and 3800) were involved in the protein−ligand activity of all DK complexes through hydrophobic contacts as confirmed from MM-PBSA studies.

The presence of the Ala3616 residue with significant hydrophobic interactions and a negative energy contribution also facilitates effective protein−ligand binding in most of the DK complexes, especially in DK01, DK02, and DK04. Amino acid residues Leu3584 and Ala3616 identified in MM-PBSA studies were also found as interacting residues in the best docking poses earlier. However, the hydrogen bonding with amino acid residue Arg3799 (with positive energy contribution) was found to be not energetically favorable in most cases of solvated protein−ligand complexes.

Results of computational MM-PBSA protein−ligand binding energies were found to be in close agreement with in vitro studies of the cytotoxic capability and IC_{50} evaluation of DK01−DK08 conducted in human B cell leukemic cell line Nalm6 rather than in the human T cell leukemic cell line CEM. DK01−DK05 in Nalm6 demonstrated increased cell death at doses as low as 2 μM. DK07 and DK08 need a higher concentration of 100 μM for its better activity in cell lines. Based on the Nalm6 IC_{50} studies, the order of inhibitory activity of DK compounds against the probable targets in the cell line was given as DK04 ≈ DK05 > DK02 > DK01 ≈ DK03. When results from two cell lines were taken into consideration, DK04 and DK05 demonstrated superior

https://doi.org/10.1021/acsomega.3c05816
ACS Omega 2023, 8, 38619−38631

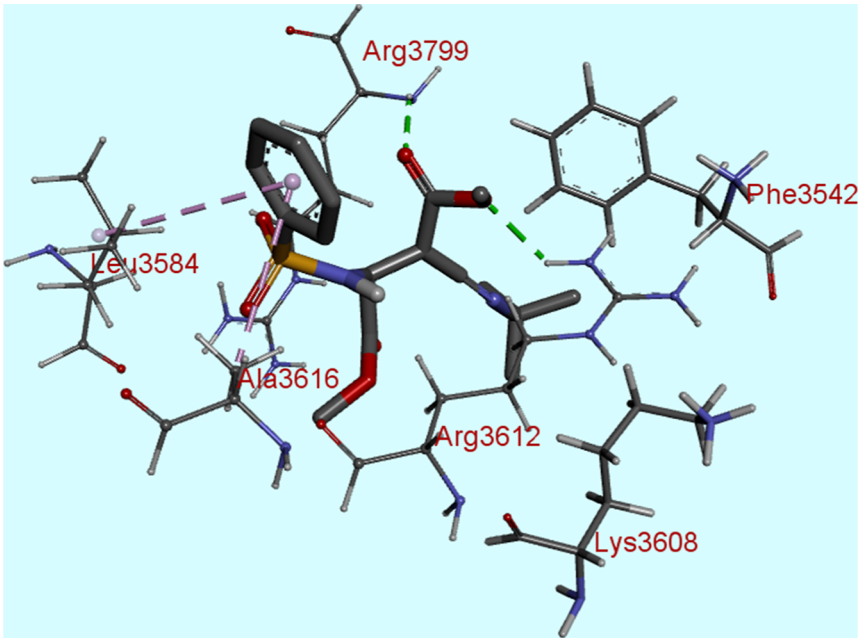

Figure 6. 3D representation of the best docking pose highlighting the interactions between the DK01 compound (stick representation) and active site amino acid residues (ball and stick representation) of the protein kinase.

Table 3. Dock Score and IC_{50} Values of DK01−DK08

compound name	dock score (kcal/mol)	IC_{50} value (μM) in Nalm6 (48 h)	IC_{50} value (μM) in Cem (48 h)
DK01	−8.5	11.04	92.63
DK02	−8.5	8.11	38.16
DK03	−8.7	11.27	50.71
DK04	−8.8	2.80	41.76
DK05	−8.8	2.57	24.43
DK06	−8.4	17.84	23.43
DK07	−8.4	86.20	94.83
DK08	−8.2	143.95	50.60

cytotoxicity in both cells. The potential exhibited by DK04 and DK05 compounds with closer binding energy values as the best inhibitors of kinase target (probable target included in the Nalm6 cell line) was also confirmed and validated from the computational MM-PBSA binding energy calculations. MM-PBSA binding energies and comparative inhibition of all other DK series obtained from the in silico studies closely matched the trends observed in Nalm6 IC_{50}investigations.

3. CONCLUSIONS

We have synthesized a series of analogous small molecules by a highly atom economical synthetic route. All the molecules were obtained in crystalline form, yielding a single stereo isomer. Biological evaluation through cytotoxic studies revealed the potential of these compounds as anticancer agents. Specifically, bromo- and nitro-substituted ketenimine sulfonamides (DK04 and DK05, respectively) were found to have excellent IC_{50} values in the low micromolar range against Nalm6 cell lines. The substituent effect of halogen atoms on benzene shows that only bromine substitution makes the molecule effective against the Nalm6 cell line. Nitro substitution also showed equal activity by cytotoxic and computational evaluation. Molecular docking and simulation experiments were found to be in agreement with the observed biological activity. The docking scores and cytotoxicity results demonstrated a consistent relationship, indicating that DK04 and DK05 exhibited strong inhibitory activity against cancer cells (Nalm6 and Cem), which have moderate to good NHEJ efficiency and expression of DNA-PK. Future experiments to target the DNA-PK activity

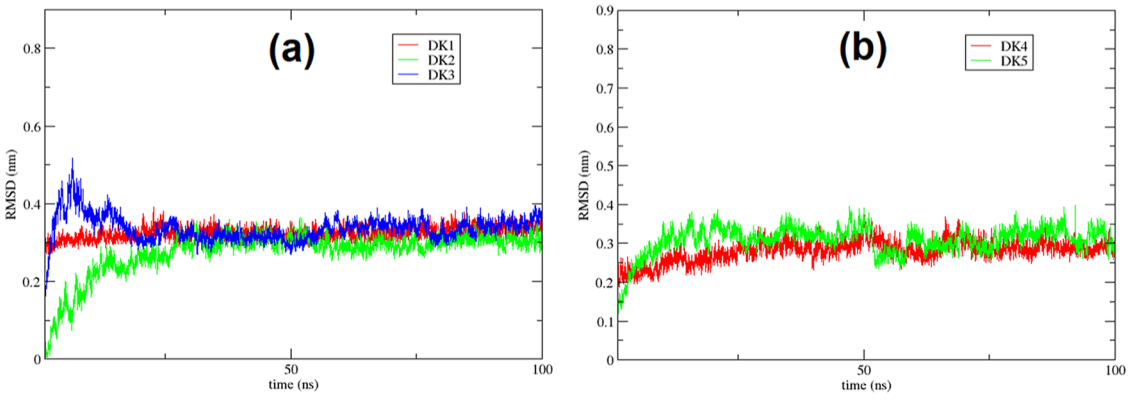

Figure 7. RMSD plots of (a) DK01−DK03 complex structures and (b) DK04−DK05 complex structures in the MD trajectory.

https://doi.org/10.1021/acsomega.3c05816
ACS Omega 2023, 8, 38619−38631

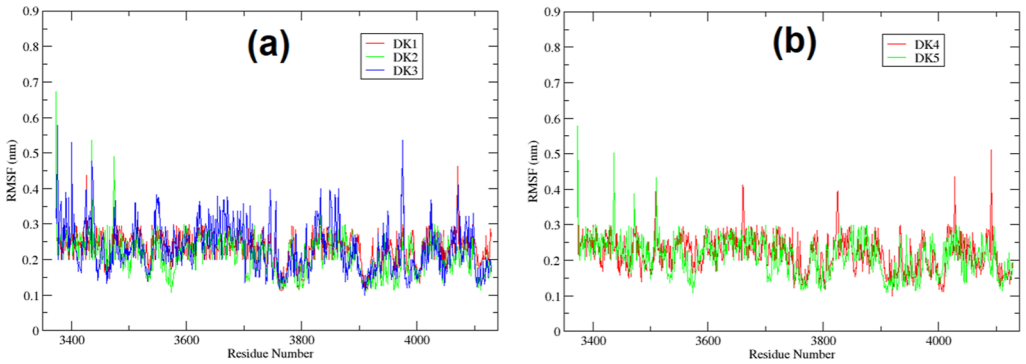

Figure 8. RMSF of protein residues in (a) DK01−DK03 complexes and (b) DK04−DK05 complexes in the MD trajectory.

Table 4. MM-PBSA Binding Energies with Standard Deviations of DK Protein−Ligand Complexes and Subcomponents of the Net MM-PBSA Binding Energy

ketenimine complex	van der Waal energy (kJ/mol)	electrostatic energy (kJ/mol)	polar solvation energy (kJ/mol)	SASA energy (nonpolar solvation) (kJ/mol)	binding energy (kJ/mol)
DK01	−219.582	−42.74	185.273	−23.675	−100.725 ± 9.47
DK02	−204.518	−64.916	201.944	−21.276	−88.765 ± 10.2
DK03	−223.953	−33.69	175.15	−23.067	−105.56 ± 10.4
DK04	−201.073	−58.629	161.212	−21.208	−119.699 ± 10.6
DK05	−228.643	−112.832	252.383	−21.933	−111.025 ± 9.1
DK06	−234.598	−49.961	220.931	−23.782	−87.409 ± 8.2
DK07	−109.717	−3.751	48.225	−12.326	−77.569 ± 10.34
DK08	−182.66	−69.514	201.06	−21.103	−72.217 ± 9.34

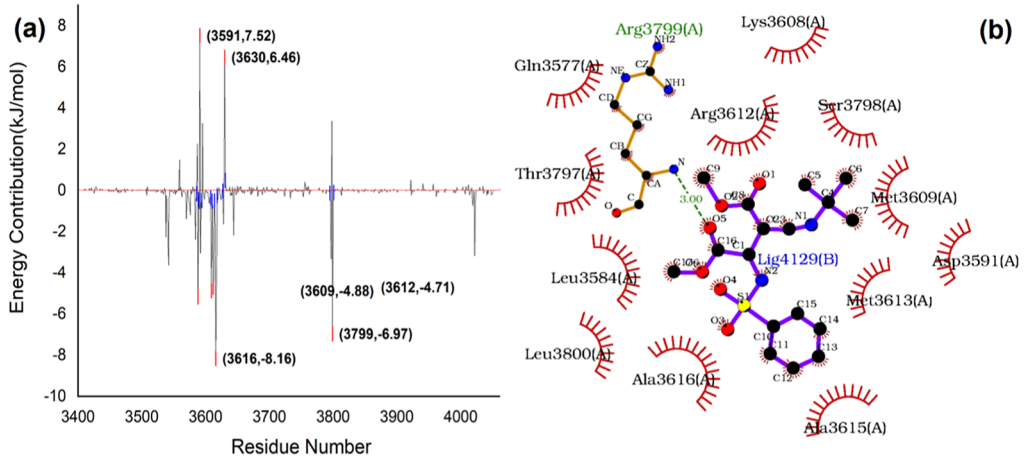

Figure 9. (a) Significant hot spot and bad contact (residue id's) with negative and positive energy contributions, respectively, to the total MM-PBSA binding energy of the DK01 complex. (b) Corresponding nonbonding interaction profile between the DK01 ligand residue and protein residues in its complex structure. Among these residues, the id of DK01−ligand residue is Lig4129 (b). Protein residues exhibiting hydrophobic and hydrogen bonded interactions with the ligand are labeled by red arcs and ball/stick representation with green dotted lines, respectively.

need to be done to reiterate the potential of these derivatives as anticancer agents.

4. EXPERIMENTAL METHODS

4.1. Materials and Methods. The purity was determined by high-performance liquid chromatography (HPLC). Purity of all final compounds was found to be 95% or higher. A Shimadzu semipreparative HPLC instrument [SPD-M10A UV-detector)] was used. A Thermoscientific C18, 5 μm particle size (250 mm × 4.6 mm) column was employed. HPLC analysis of all compounds was performed by eluent A, acetonitrile; eluent B, water, binary MeCN/H_2O = 90/10 to 10/90; flow rate = 1.0 mL/min; detection at 254 nm; column temperature of 25 °C; and injection of 20 μL of 34.3 mM DK series in methanol. Mass spectra were recorded on a Waters SYNAPT-G2 equipped with a Waters Z-spray ESI source. ^{1}H NMR and ^{13}C NMR spectra were recorded on a BRUKER 400 MHz and JEOL 400 MHz spectrometer. NMR spectra were obtained on solutions in $CDCI_3$. The chemicals used in this work were purchased from Sigma-Aldrich. HPLC grade dichloromethane (DCM) was used as the solvent for the reaction.

4.2. Procedure. The typical procedure for the synthesis of ketenimines DK01 to DK08 is as follows: To a stirred solution of benzenesulfonamide derivatives (2.5 mmol) and dimethyl acetylene dicarboxylate (2.5 mmol), tertiary-butyl isocyanide (2.5 mmol) was added. The mixture was stirred for 8 to 12 h in

https://doi.org/10.1021/acsomega.3c05816
ACS Omega 2023, 8, 38619−38631

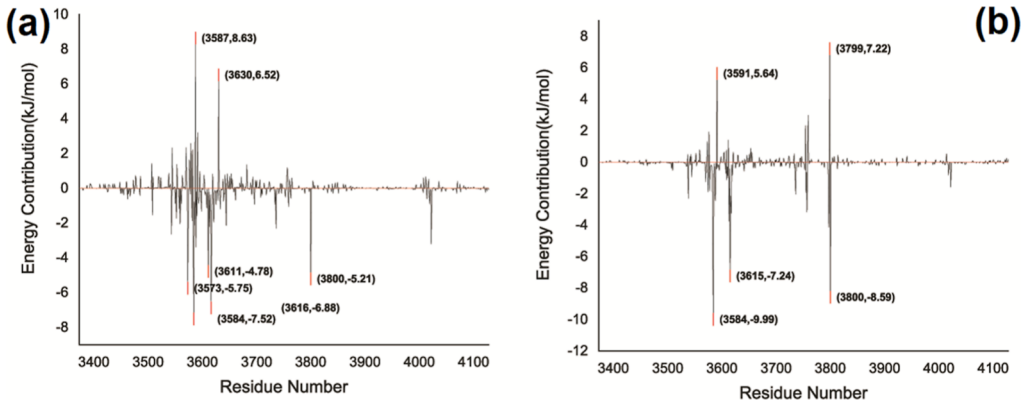

Figure 10. Significant hot spot and bad contact residue id's with its energy value contributions, respectively, to the total MM-PBSA binding energy of (a) DK02 and (b) DK03 complexes.

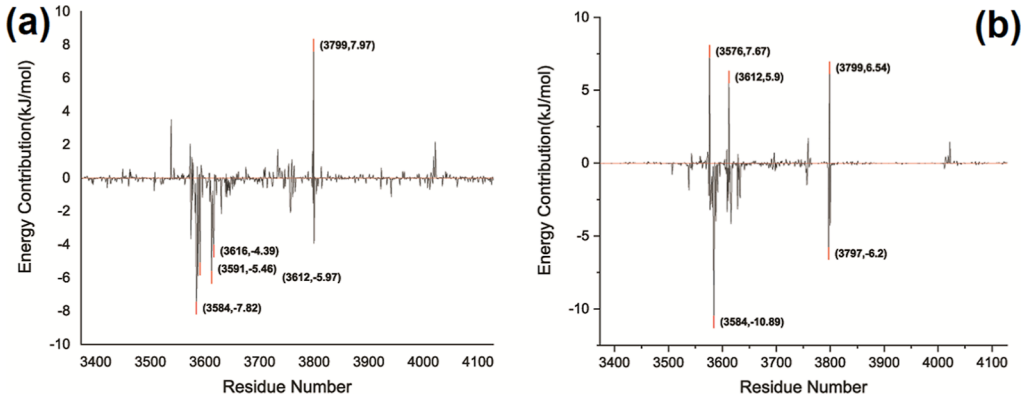

Figure 11. Significant hot spot and bad contact residue id's with their energy value contributions, respectively, to the total MM-PBSA binding energy of (a) DK04 and (b) DK05 complexes.

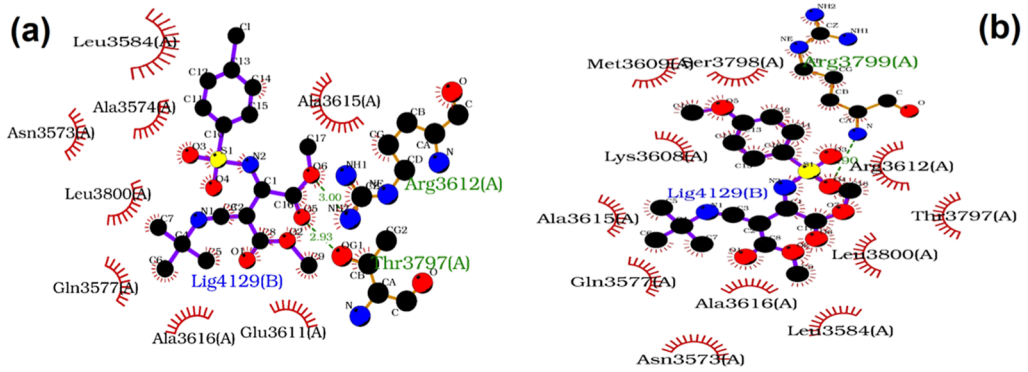

Figure 12. Nonbonding interaction between ligand residue and protein residues in (a) DK02 and (b) DK03 complexes. Protein residues exhibiting hydrophobic and hydrogen bonded interactions with the ligand are shown by red arcs and ball/stick representation with green dotted lines, respectively.

20 mL of DCM. DCM was removed under reduced pressure, and the product was recrystallized from a 2:1 (vol/vol) methanol−ethanol mixture.[42] The crystals were washed with methanol and dried under vacuum.

4.3. Dimethyl 2-((*tert*-Butylimino)methylene)-3-(phenylsulfonamido)succinate (DK01). White crystalline solid; 80% yield (0.76392 g, 1.99 mmol). ^{1}H NMR (CDCl3, 400 MHz): δ_H (ppm) 1.35 (9H, s, $C(CH_3)_3$, 3.54 (6H, m, 2 × OCH_3), 4.61 (1H, d, ^3J = 8.0 Hz, CHNH), 5.76 (1H, d, ^3J = 8.0 Hz), 7.40−7.51 (m, 3H, arom), 7.78−7.81(m, 2H, arom). δc (ppm) 29.4, 50.6, 52.1, 52.7, 61.9, 62.6, 126.1, 127.9, 131.6, 139.3, 164.6, 167.8, 168.9. HRMS $(M + Na)^+$ $C_{17}H_{22}N_2NaO_6S$ 405.1096 (Calcd); 405.1083.

4.4. Dimethyl 2-((*tert*-Butylimino)methylene)-3-(4-chlorophenylsulfonamido)succinate (DK02). White crystalline solid; 79% yield (0.8224 g, 1.97 mmol), ^{1}H NMR (CDCl3, 400 MHz): δ_H (ppm) 1.35 (9H, s, $C(CH_3)_3$), 3.55−3.59 (6H, m, 2 × OCH_3), 4.60 (1H, d, $^3J_{HH}$ = 8.0 Hz), 5.80 (m, 1H), 7.38−7.40 (m, 2H, arom), 7.72−7.74 (m, 2H, arom). δc (ppm): 30.4, 51.7, 53.2, 53.8, 63.0, 63.3, 128.6, 129.1, 139.1, 165.3, 168.7, 169.8. HRMS $(M + Na)^+$ $C_{17}H_{21}ClN_2NaO_6S$ 439.0707 (Calcd); 439.0714.

https://doi.org/10.1021/acsomega.3c05816
ACS Omega 2023, 8, 38619−38631

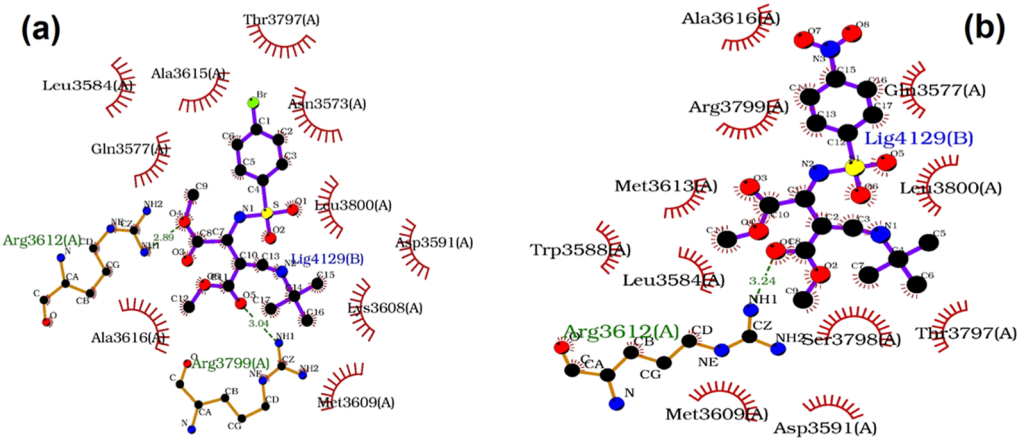

Figure 13. Nonbonding interaction between ligand residue and protein residues in (a) DK04 and (b) DK05 complexes. Protein residues exhibiting hydrophobic and hydrogen bonded interactions with the ligand are shown by red arcs and ball/stick representation with green dotted lines, respectively.

4.5. Dimethyl 2-((*tert*-Butylimino)methylene)-3-(4-methoxyphenylsulfonamido)succinate (DK03). White crystalline solid; 80% yield (0.824 g, 2 mmol), ^{1}H NMR (CDCl3, 400 MHz): δ_H (ppm) 1.43 (9H, s, C$(CH_3)_3$), 3.63 (6H, m, 2 × OCH_3), 3.86 (CH_3), 4.63 (1H, d, $^3J_{HH}$ = 8.0 Hz), 5.74 (m, 1H), 6.94−6.96 (m, 2H, arom), 7.78−7.80 (m, 2H, arom). δc (ppm): 30.5, 51.8, 53.2, 53.6, 56.0, 63.0, 63.9, 114.1, 129.4, 131.9, 160.0, 168.9, 170.2. HRMS (M + H)$^+$ $C_{18}H_{25}N_2O_7S$ 413.1382 (Calcd); 413.0657

4.6. Dimethyl 2-((*tert*-Butylimino)methylene)-3-(4-bromophenylsulfonamido)succinate (DK04). White crystalline solid; 75% yield (0.864 g, 1.88 mmol), ^{1}H NMR (CDCl3, 400 MHz): δ_H (ppm) 1.41 (9H, s, C$(CH_3)_3$), 3.60−3.65 (6H, m, 2 × OCH_3), 4.64 (1H, d, $^3J_{HH}$ = 8.0 Hz), 5.85 (m, 1H), 7.60−7.62 (m, 2H, arom), 7.70−7.72 (m, 2H, arom). δc (ppm): 30.5, 51.8, 53.3, 53.8, 63.1, 63.4, 127.7, 128.8, 132.2, 139.6, 165.3, 168.9, 169.9. HRMS (M + H)$^+$ $C_{17}H_{22}BrN_2O_6S$ 461.0382 (Calcd); 461.9653

4.7. Dimethyl 2-((*tert*-Butylimino)methylene)-3-(4-nitrophenylsulfonamido)succinate (DK05). White crystalline solid; 75% yield (0.8002 g, 1.87 mmol), ^{1}H NMR (CDCl3, 400 MHz): δ_H (ppm) 1.43 (9H, s, C$(CH_3)_3$), 3.60−3.68 (6H, m, 2 × OCH_3), 4.73 (1H, d, $^3J_{HH}$ = 8.0 Hz), 6.08 (m, 1H), 8.07−8.04 (m, 2H, arom), 8.34−8.32 (m, 2H, arom). δc (ppm) 30.4, 51.8, 53.3, 54.0, 62.9, 63.2, 124.1, 128.4, 146.5, 150.0, 164.6, 168.8, 169.5. HRMS (M + H)$^+$ $C_{17}H_{22}N_3O_8S$ 428.1128 (Calcd); 428.1118

4.8. Dimethyl 2-((*tert*-Butylimino)methylene)-3-(4-isopropylphenylsulfonamido)succinate (DK06). White crystalline solid; 75% yield (0.795 g, 1.875 mmol). ^{1}H NMR (CDCl3, 400 MHz): δ_H (ppm) 1.25 (6H, s, 2 × CH_3), 1.40 (9H, s, C$(CH_3)_3$), 2.93 (1H, q, CH), 3.60 (6H, s, 2 x OCH_3), 4.64 (1H, d, $^3J_{HH}$ = 8.0 Hz), 5.77 (1H, d), 7.30−7.32 (m, 2H, arom), 7.74−7.77 (m, 2H, arom). δc (ppm): 23.8, 30.5, 34.3, 51.8, 53.2, 53.7, 63.0, 63.8, 127.1, 127.4, 137.6, 154.1, 165.9, 168.9, 170.1. HRMS (M + Na)$^+$ $C_{20}H_{28}N_2NaO_6S$ 447.1566 (Calcd); 447.1570.

4.9. Dimethyl 2-((*tert*-Butylimino)methylene)-3-(4-fluorophenylsulfonamido)succinate (DK07). White crystalline solid; 75% yield (0.6199 g, 1.55 mmol). ^{1}H NMR (CDCl3, 400 MHz): δ_H (ppm) 1.41 (9H, s, C$(CH_3)_3$), 3.61 (s, 3H, OCH_3), 3.65 (s, 3H, OCH_3) 4.65 (1H, d, $^3J_{HH}$ = 8.0 Hz), 5.81 (m, 1H), 7.13−7.17 (m, 2H, arom), 7.85−7.88 (m, 2H, arom). δc (ppm) 30.5, 51.8, 53.3, 53.8, 63.1, 63.5, 116.1, 116.3, 130.0, 136.6, 165.5, 168.9, 168.9, 169.9. HRMS (M + Na)$^+$ $C_{17}H_{21}FN_2NaO_6S$ 423.1002 (Calcd); 423.1013.

4.10. Dimethyl 2-((*tert*-Butylimino)methylene)-3-(4-iodophenylsulfonamido)succinate (DK08). White crystalline solid; 54% yield (0.6831 g, 1.34 mmol). ^{1}H NMR ($CDCl_3$, 400 MHz): δ_H (ppm) 1.41 (9H, s, C$(CH_3)_3$), 3.61 (s, 3H, OCH_3), 3.65 (s, 3H, OCH_3) 4.64 (1H, d, $^3J_{HH}$ = 8.0 Hz), 5.83 (m, 1H), 7.55−7.57 (m, 2H, arom), 7.81−7.84 (m, 2H, arom). δc (ppm): 30.5, 51.8, 53.3, 53.8, 63.1, 63.4, 100.1, 128.7, 138.2, 140.2, 165.3, 168.9, 169.8. HRMS (M + Na)$^+$$C_{17}H_{21}IN_2NaO_6S$ 531.0063 (Calcd); 531.0071.

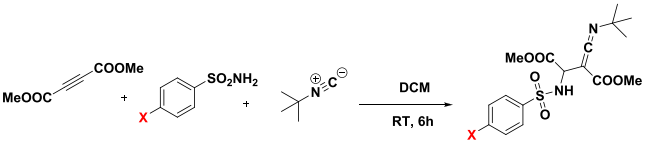

R_2	-H (DK01)	-Cl (DK02)	-OCH_3 (DK03)	-Br (DK04)	-NO_2 (DK05)	$CH(CH_3)_2$ (DK06)	-F (DK07)	-I (DK08)
Yield (%)	80	79	80	75	75	75	62	54

4.11. Cell Lines and Culture Media. Human B cell leukemia cell line, Nalm6, and human T cell leukemic cell line, CEM were cultured in RPMI 1640 supplemented with 10% FBS and 100 U of penicillin G/mL and 100 mg/mL of streptomycin, as described before.[28,59−61]

4.12. Cytotoxicity Analysis by Trypan Blue Exclusion Assay. Cytotoxicity analyses of DK compounds were performed using trypan blue assay, as described before.[28,62,63] Briefly, 25,000 cells/mL were seeded in 24-well tissue culture grade plates and treated with increasing concentrations of the compounds DK01−DK08 (1, 2, 5, 10, 50, 100 μM) for 48 h. The control cells were treated with an equivalent highest concentration of DMSO. After 48 h of incubation, cells were mixed in a 1:1 ratio in 0.4% Trypan Blue (Sigma-Aldrich, USA) prepared in 1× PBS and counted under a microscope using a hemo cytometer. Viable cells that did not take up the stain were counted and represented in percentage as a function of concentration.

https://doi.org/10.1021/acsomega.3c05816
ACS Omega 2023, 8, 38619−38631

The 50% inhibitory concentration or IC_{50} of DK01−DK08 was calculated at 48 h using GraphPad Prism software. Experiments were performed minimum thrice independently, and error bars denote mean ± SEM.

4.13. Materials and Methods in Computational Calculations. *4.13.1. Molecular Docking Calculations.* The ketenimine series were docked to Chain C of DNA-dependent kinase protein (PDB ID; 5Y3R). The catalytic amino acid residues belong to this region. B3LYP-SVP-optimized geometries of ketenimine compounds obtained from Turbomole software (Quantum-DFT package) were used in complete in silico studies. Autodock Vina version 1.2 package was utilized to execute the molecular docking calculations.[17,64−66] The binding site domain of the kinase C is documented in the literature. The center of the grid box in the vina calculation is fixed at the centroid of this binding site domain located between AMN3676 and AMN4100 of the protein kinase. There are 4600 grid points in the vina calculation. The exhaustiveness parameter was set to a default value of 8. The protein−ligand complex structures (docking poses) corresponding to higher docking scores are selected for analysis and further simulation studies.

4.13.2. Molecular Dynamics Simulations. Protein−ligand molecular dynamics simulations of 9 ketenimine−kinase complexes were performed using the GROMACS 2018.1 package. The best docking poses obtained from the molecular docking calculations were used as the initial structures for the MD simulations. Each docked ligand was protonated at physiological P^H and uploaded to the ATB server to obtain the GROMOS force field parameters for both ligand and protein systems. The protein ligand complex structure is solvated using TIP3P water molecules in a cubic periodic box followed by energy minimization using the steepest descent method. Two ns's *NVT* and *NPT* equilibration were performed prior to 100 ns of production run. Temperature and pressure of the simulating system were controlled at 310 K and 1 bar, respectively. The Verlet algorithm was used for integration with a time step of 2 fs. The bond constraints and electrostatic interactions were dealt with linear constraint solver (LINCS) and particle−mesh Ewald algorithms, respectively. The coordinates of the MD trajectory obtained during the production run were saved after every 10 ps. In order to validate the consistency of results from the MD trajectory and post MD MM-PBSA calculations, we performed short-duration MD replicates followed by trajectory analysis.

4.13.3. MM-PBSA Binding Free Energy Calculations. We have utilized the g_mmpbsa code implemented with MM-PBSA binding free energy calculations to find the binding affinity of ketenimines in all its complexes with the kinase protein.[67] We have utilized the protein−ligand conformations from the equilibrated MD trajectory to perform these calculations.[68] The free energy (G) of binding a ligand (L) to a protein (P) to form a protein−ligand complex (C) is calculated as

$$\Delta G_{bind} = G_C - (G_P + G_L) \quad (1)$$

Generally, the G term is calculated as

$$G = E_{MM} + G_{solv} - TS \quad (2)$$

$$E_{MM} = E_{bonded} + E_{elec} + E_{vdW} \quad (3)$$

The molecular mechanics potential (E_{MM}) in eq 3 is obtained by adding bonding and nonbonding terms, where the latter includes van der Waals and electrostatic terms. In the current methodology of finding the relative binding energy, the entropy term (TS) in eq 2 is neglected.

$$G_{solv} = G_{PB} + G_{SA} \quad (4)$$

The free energy of solvation (G_{solv}) is the sum of Poisson−Boltzmann Equation (G_{PB}) term of polar interactions and nonpolar free energy term (G_{SA}) of solvent-accessible surface area. The solvent dielectric constant and solvent probe radius were set as 80 and 1.4 Å, respectively, in the MM-PBSA calculation. The binding free energies of protein−ligand systems obtained from these calculations were further validated by repeating the same using protein−ligand conformations obtained from MD replicates. Further, we also analyzed the crucial residues of complex systems that contributed to the MM-PBSA binding energy using "energyb2fac" code, which performed the binding energy decomposition analysis.

■ ASSOCIATED CONTENT

Supporting Information

The Supporting Information is available free of charge at https://pubs.acs.org/doi/10.1021/acsomega.3c05816.

HPLC, ^{1}HNMR, ^{13}CNMR, and HRMS spectra of DK01 to DK08, docking score corresponding to the best DK inhibitor with high binding affinity of the target, 3D Cartesian coordinates of DK compounds used in computational docking calculations, docking results of DK compounds with target proteins of the NHEJ pathway, and best docking poses highlighting nonbonding interactions between DK compounds and active site amino acid residues of the DNA-PK target (5y3r-ChainC) (PDF)

■ AUTHOR INFORMATION

Corresponding Author

Franklin John − *Post Graduate and Research Department of Chemistry, Sacred Heart college (M.G University), Thevara, Kerala 682013, India;* orcid.org/0000-0002-3340-0858; Email: frank89ind@yahoo.com

Authors

Deepak J. Prabhu − *Post Graduate Research Department of Chemistry, Maharajas College, Ernakulam, Ernakulam, Kerala 682011, India*

Ujjayinee Ray − *Department of Microbiology, Techno India University, Kolkata, West Bengal 700091, India*

Anjaly Rajeev − *Post Graduate and Research Department of Chemistry, Sacred Heart college (M.G University), Thevara, Kerala 682013, India*

Reshma Joy − *Post Graduate and Research Department of Chemistry, Sacred Heart college (M.G University), Thevara, Kerala 682013, India*

Abi Thoppilan George − *Post Graduate and Research Department of Chemistry, Sacred Heart college (M.G University), Thevara, Kerala 682013, India;* orcid.org/0000-0002-5915-8609

Jinu George − *Post Graduate and Research Department of Chemistry, Sacred Heart college (M.G University), Thevara, Kerala 682013, India;* orcid.org/0000-0002-8802-6760

Sathees C. Raghavan − *Department of Biochemistry, Indian Institute of Science, Bengaluru 560012, India*

Complete contact information is available at:

https://doi.org/10.1021/acsomega.3c05816
ACS Omega 2023, 8, 38619−38631

https://pubs.acs.org/10.1021/acsomega.3c05816

Funding
Reshma Joy acknowledges the Government of Kerala for a research fellowship. Dr. Franklin John acknowledges Kairali Research Award (2020) from the Kerala State Higher Education Council, Government of Kerala.

Notes
The authors declare no competing financial interest.

■ ACKNOWLEDGMENTS

We acknowledge the laboratory facility and support from Sacred Heart College, Thevara, Kochi, India.

■ ABBREVIATIONS

CCR2, CC chemokine receptor 2; CCL2, CC chemokine ligand 2; CCR5, CC chemokine receptor 5; TLC, thin-layer chromatography

■ REFERENCES

(1) Sung, H.; Ferlay, J.; Siegel, R. L.; Laversanne, M.; Soerjomataram, I.; Jemal, A.; Bray, F. Global Cancer Statistics 2020: GLOBOCAN Estimates of Incidence and Mortality Worldwide for 36 Cancers in 185 Countries. *Ca-Cancer J. Clin.* **2021**, *71* (3), 209−249.
(2) Jemal, A.; Thun, M. J.; Ries, L. A. G.; Howe, H. L.; Weir, H. K.; Center, M. M.; Ward, E.; Wu, X.-C.; Eheman, C.; Anderson, R.; Ajani, U. A.; Kohler, B.; Edwards, B. K. Annual Report to the Nation on the Status of Cancer, 1975−2005, Featuring Trends in Lung Cancer, Tobacco Use, and Tobacco Control. *JNCI, J. Natl. Cancer Inst.* **2008**, *100* (23), 1672−1694.
(3) Harris, A. L.; Hochhauser, D. Mechanisms of Multidrug Resistance in Cancer Treatment. *Acta Oncol.* **1992**, *31* (2), 205−213.
(4) Ray, U.; John, F.; Pooppadi, S.; George, J.; Sharma, S.; Raghavan, S. C. Novel Synthetic Aromatic Thiourea Derivatives and Investigations on Their Cytotoxic Potential Efficacy. *J. Heterocycl. Chem.* **2021**, *58* (1), 40−47.
(5) Nambiar, M.; Raghavan, S. C. Chromosomal Translocations among the Healthy Human Population: Implications in Oncogenesis. *Cell. Mol. Life Sci.* **2013**, *70*, 1381−1392.
(6) Roy, U.; Raghavan, S. C. Deleterious Point Mutations in T-Cell Acute Lymphoblastic Leukemia: Mechanistic Insights into Leukemogenesis. *Int. J. Cancer* **2021**, *149* (6), 1210−1220.
(7) Guo, Z.; Mohanty, U.; Noehre, J.; Sawyer, T. K.; Sherman, W.; Krilov, G. Probing the α-Helical Structural Stability of Stapled P53 Peptides: Molecular Dynamics Simulations and Analysis. *Chem. Biol. Drug Des.* **2010**, *75* (4), 348−359.
(8) Dörrie, J.; Gerauer, H.; Wachter, Y.; Zunino, S. J. Resveratrol Induces Extensive Apoptosis by Depolarizing Mitochondrial Membranes and Activating Caspase-9 in Acute Lymphoblastic Leukemia Cells1. *Cancer Res.* **2001**, *61* (12), 4731−4739.
(9) Protein Data Bank. RCSB PDB—3W5O: Crystal Structure of Human DNA ligase IV. https://www.rcsb.org/structure/3w5o (accessed 2022-07-03).
(10) Protein Data Bank. RCSB PDB—1JEY: Crystal Structure of the Ku heterodimer bound to DNA. https://www.rcsb.org/structure/1JEY (accessed 2022-07-03).
(11) Inagawa, T.; Wennink, T.; Lebbink, J. H. G.; Keijzers, G.; Florea, B. I.; Verkaik, N. S.; van Gent, D. C. C-Terminal Extensions of Ku70 and Ku80 Differentially Influence DNA End Binding Properties. *Int. J. Mol. Sci.* **2020**, *21* (18), 6725.
(12) Junop, M. S.; Modesti, M.; Guarné, A.; Ghirlando, R.; Gellert, M.; Yang, W. Crystal Structure of the Xrcc4 DNA Repair Protein and Implications for End Joining. *EMBO J.* **2000**, *19* (22), 5962−5970.
(13) Wu, P.-Y.; Frit, P.; Meesala, S.; Dauvillier, S.; Modesti, M.; Andres, S. N.; Huang, Y.; Sekiguchi, J.; Calsou, P.; Salles, B.; et al. Structural and Functional Interaction between the Human DNA Repair Proteins DNA Ligase IV and XRCC4. *Mol. Cell. Biol.* **2009**, *29* (11), 3163−3172.
(14) Protein Data Bank. RCSB PDB—1IK9: Crystal Structure Of A XRCC4-DNA Ligase IV Complex. https://www.rcsb.org/structure/1ik9 (accessed accessed 2022-07-04).
(15) Hammel, M.; Rey, M.; Yu, Y.; Mani, R. S.; Classen, S.; Liu, M.; Pique, M. E.; Fang, S.; Mahaney, B. L.; Weinfeld, M.; et al. XRCC4 Protein Interactions with XRCC4-like Factor (XLF) Create an Extended Grooved Scaffold for DNA Ligation and Double Strand Break Repair. *J. Biol. Chem.* **2011**, *286* (37), 32638−32650.
(16) Yosaatmadja, Y.; Baddock, H. T.; Newman, J. A.; Bielinski, M.; Gavard, A. E.; Mukhopadhyay, S. M.; Dannerfjord, A. A.; Schofield, C. J.; McHugh, P. J.; Gileadi, O. Structural and Mechanistic Insights into the Artemis Endonuclease and Strategies for Its Inhibition. *Nucleic Acids Res.* **2021**, *49* (16), 9310−9326.
(17) Yin, X.; Liu, M.; Tian, Y.; Wang, J.; Xu, Y. Cryo-EM Structure of Human DNA-PK Holoenzyme. *Cell Res.* **2017**, *27* (11), 1341−1350.
(18) Davis, A. J.; Chen, D. J. DNA Double Strand Break Repair via Non-Homologous End-Joining. *Transl. Cancer Res.* **2013**, *2* (3), 130−143.
(19) Lieber, M. R. The Mechanism of Double-Strand DNA Break Repair by the Nonhomologous DNA End Joining Pathway. *Annu. Rev. Biochem.* **2010**, *79*, 181−211.
(20) Raghavan, S. C.; Lieber, M. R. Chromosomal Translocations and Non-B DNA Structures in the Human Genome. *Cell Cycle* **2004**, *3* (6), 760−766.
(21) Ray, U.; Raghavan, S. C. Inhibitors of DNA Double-Strand Break Repair at the Crossroads of Cancer Therapy and Genome Editing. *Biochem. Pharmacol.* **2020**, *182*, 114195.
(22) Ray, U.; Raghavan, S. C. Modulation of DNA Double-Strand Break Repair as a Strategy to Improve Precise Genome Editing. *Oncogene* **2020**, *39* (41), 6393−6405.
(23) Ghosh, D.; Raghavan, S. C. Nonhomologous End Joining: New Accessory Factors Fine Tune the Machinery. *Trends Genet.* **2021**, *37* (6), 582−599.
(24) Srivastava, M.; Raghavan, S. C. DNA Double-Strand Break Repair Inhibitors as Cancer Therapeutics. *Chem. Biol.* **2015**, *22* (1), 17−29.
(25) Joensuu, H.; Roberts, P. J.; Sarlomo-Rikala, M.; Andersson, L. C.; Tervahartiala, P.; Tuveson, D.; Silberman, S. L.; Capdeville, R.; Dimitrijevic, S.; Druker, B.; et al. Effect of the Tyrosine Kinase Inhibitor STI571 in a Patient with a Metastatic Gastrointestinal Stromal Tumor. *N. Engl. J. Med.* **2001**, *344* (14), 1052−1056.
(26) Manley, P. W.; Cowan-Jacob, S. W.; Buchdunger, E.; Fabbro, D.; Fendrich, G.; Furet, P.; Meyer, T.; Zimmermann, J. Imatinib: A Selective Tyrosine Kinase Inhibitor. *Eur. J. Cancer* **2002**, *38*, S19−S27.
(27) Yue, X.; Bai, C.; Xie, D.; Ma, T.; Zhou, P.-K. DNA-PKcs: A Multi-Faceted Player in DNA Damage Response. *Front. Genet.* **2020**, *11*, 607428.
(28) Srivastava, M.; Nambiar, M.; Sharma, S.; Karki, S. S.; Goldsmith, G.; Hegde, M.; Kumar, S.; Pandey, M.; Singh, R. K.; Ray, P.; et al. An Inhibitor of Nonhomologous End-Joining Abrogates Double-Strand Break Repair and Impedes Cancer Progression. *Cell* **2012**, *151* (7), 1474−1487.
(29) Ray, U.; Raghavan, S. C. Understanding the DNA Double-Strand Break Repair and Its Therapeutic Implications. *DNA Repair* **2021**, *106*, 103177.
(30) Massaro, N. P.; Chatterji, A.; Sharma, I. Three-Component Approach to Pyridine-Stabilized Ketenimines for the Synthesis of Diverse Heterocycles. *J. Org. Chem.* **2019**, *84* (21), 13676−13685.
(31) Lu, P.; Wang, Y. The thriving chemistry of ketenimines. *Chem. Soc. Rev.* **2012**, *41*, 5687.
(32) Alajarin, M.; Marin-Luna, M.; Vidal, A. Recent Highlights in Ketenimine Chemistry. *Eur. J. Org Chem.* **2012**, *2012* (29), 5637−5653.
(33) Yang, Y.-Y.; Shou, W.-G.; Hong, D.; Wang, Y.-G. Selective Synthesis of 4-Alkylidene-β-Lactams and N,N′-Diarylamidines from

Azides and Aryloxyacetyl Chlorides via a Ketenimine-Participating One-Pot Cascade Process. *J. Org. Chem.* **2008**, *73* (9), 3574−3577.
(34) Fromont, C.; Masson, S. Reactivity of N-Phenyl Silylated Ketenimines with Electrophilic Reagents. *Tetrahedron* **1999**, *55* (17), 5405−5418.
(35) Bendikov, M.; Duong, H. M.; Bolanos, E.; Wudl, F. An Unexpected Two-Group Migration Involving a Sulfonynamide to Nitrile Rearrangement. Mechanistic Studies of a Thermal N → C Tosyl Rearrangement. *Org. Lett.* **2005**, *7* (5), 783−786.
(36) Bae, I.; Han, H.; Chang, S. Highly Efficient One-Pot Synthesis of N-Sulfonylamidines by Cu-Catalyzed Three-Component Coupling of Sulfonyl Azide, Alkyne, and Amine. *J. Am. Chem. Soc.* **2005**, *127* (7), 2038−2039.
(37) Váradi, A.; Palmer, T. C.; Notis Dardashti, R.; Majumdar, S. Isocyanide-Based Multicomponent Reactions for the Synthesis of Heterocycles. *Molecules* **2016**, *21* (1), 19.
(38) Zhu, J.; Bienaymé, H. *Multicomponent Reactions*; John Wiley & Sons, 2006.
(39) José Climent, M.; Corma, A.; Iborra, S. Homogeneous and Heterogeneous Catalysts for Multicomponent Reactions. *RSC Adv.* **2012**, *2* (1), 16−58.
(40) Ruijter, E.; Orru, R. Multicomponent Reactions in Drug Discovery and Medicinal Chemistry. *Drug Discovery Today: Technol.* **2018**, *29*, 1−2.
(41) Weber, L. The Application of Multi-Component Reactions in Drug Discovery. *Curr. Med. Chem.* **2002**, *9* (23), 2085−2093.
(42) Xiong, Q.; Dong, S.; Chen, Y.; Liu, X.; Feng, X. Asymmetric Synthesis of Tetrazole and Dihydroisoquinoline Derivatives by Isocyanide-Based Multicomponent Reactions. *Nat. Commun.* **2019**, *10* (1), 2116.
(43) Arya, J. S.; Joseph, M. M.; Sherin, D. R.; Nair, J. B.; Manojkumar, T. K.; Maiti, K. K. Exploring Mitochondria-Mediated Intrinsic Apoptosis by New Phytochemical Entities: An Explicit Observation of Cytochrome c Dynamics on Lung and Melanoma Cancer Cells. *J. Med. Chem.* **2019**, *62* (17), 8311−8329.
(44) Habashita, H.; Kokubo, M.; Hamano, S.; Hamanaka, N.; Toda, M.; Shibayama, S.; Tada, H.; Sagawa, K.; Fukushima, D.; Maeda, K.; et al. Design, Synthesis, and Biological Evaluation of the Combinatorial Library with a New Spirodiketopiperazine Scaffold. Discovery of Novel Potent and Selective Low-Molecular-Weight CCR5 Antagonists. *J. Med. Chem.* **2006**, *49* (14), 4140−4152.
(45) Ramos-Tomillero, I.; Pérez-Chacon, G.; Somovilla-Crespo, B.; Sánchez-Madrid, F.; Cuevas, C.; Zapata, J. M.; Domínguez, J. M.; Rodríguez, H.; Albericio, F. From Ugi Multicomponent Reaction to Linkers for Bioconjugation. *ACS Omega* **2020**, *5* (13), 7424−7431.
(46) Supuran, C. T. Special Issue: Sulfonamides. *Molecules* **2017**, *22*, 1642.
(47) Kalgutkar, A. S.; Jones, R.; Sawant, A. Sulfonamide as an Essential Functional Group in Drug Design. *Drug Discovery*; Royal Society of Chemistry, 2010; Vol. *1*, 210.
(48) Wilden, J. D. The Sulfonamide Motif as a Synthetic Tool. *J. Chem. Res.* **2010**, *34* (10), 541−548.
(49) Edris Ameri, R.; Mohtat, B.; Alipour, E.; Rahimifard, N.; Mirza, B. In-Vitro Antibacterial and Antifungal Screening of Newly Synthesized Trifluoromethylated N-Heterocyclic Ketenimines and 1-Aza Butadiene Derivatives. *J. Chem. Health Risks* **2021**, *13*, 57.
(50) Krow, G. R. Synthesis and Reactions of Ketenimines. *Angew. Chem., Int. Ed. Engl.* **1971**, *10* (7), 435−449.
(51) Ito, Y.; Hirao, T.; Ohta, N.; Saegusa, T. Synthesis of Ketenimine via (N-Alkylimino) Acylpalladium Complex Intermediate. *Tetrahedron Lett.* **1977**, *18* (11), 1009−1012.
(52) Bayat, M.; Gheidari, D.; Mehrdad, M. Recent Advances in Synthesize Ketenimines. *Arabian J. Chem.* **2022**, *15*, 104098.
(53) Mondal, S.; Malakar, S. Synthesis of Sulfonamide and Their Synthetic and Therapeutic Applications: Recent Advances. *Tetrahedron* **2020**, *76* (48), 131662.
(54) Chin, C.; Bae, J. H.; Kim, M. J.; Hwang, J. Y.; Kim, S. J.; Yoon, M. S.; Lee, M. K.; Kim, D. W.; Chung, B. S.; Kang, C. D.; et al. Radiosensitization by Targeting Radioresistance-Related Genes with Protein Kinase A Inhibitor in Radioresistant Cancer Cells. *Exp. Mol. Med.* **2005**, *37* (6), 608−618.
(55) Shaabani, A.; Sarvary, A.; Ghasemi, S.; Rezayan, A. H.; Ghadari, R.; Ng, S. W. An Environmentally Benign Approach for the Synthesis of Bifunctional Sulfonamide-Amide Compounds via Isocyanide-Based Multicomponent Reactions. *Green Chem.* **2011**, *13* (3), 582−585.
(56) Chaplin, A. K.; Blundell, T. L. Structural Biology of Multicomponent Assemblies in DNA Double-Strand-Break Repair through Non-Homologous End Joining. *Curr. Opin. Struct. Biol.* **2020**, *61*, 9−16.
(57) Kumar, T. S.; Kari, V.; Choudhary, B.; Nambiar, M.; Akila, T. S.; Raghavan, S. C. Anti-Apoptotic Protein BCL2 down-Regulates DNA End Joining in Cancer Cells. *J. Biol. Chem.* **2010**, *285* (42), 32657−32670.
(58) Britton, S.; Chanut, P.; Delteil, C.; Barboule, N.; Frit, P.; Calsou, P. ATM Antagonizes NHEJ Proteins Assembly and DNA-Ends Synapsis at Single-Ended DNA Double Strand Breaks. *Nucleic Acids Res.* **2020**, *48* (17), 9710−9723.
(59) Srivastava, M.; Hegde, M.; Chiruvella, K. K.; Koroth, J.; Bhattacharya, S.; Choudhary, B.; Raghavan, S. C. Sapodilla Plum (Achras Sapota) Induces Apoptosis in Cancer Cell Lines and Inhibits Tumor Progression in Mice. *Sci. Rep.* **2014**, *4* (1), 6147.
(60) Thomas, E.; Gopalakrishnan, V.; Hegde, M.; Kumar, S.; Karki, S. S.; Raghavan, S. C.; Choudhary, B. A Novel Resveratrol Based Tubulin Inhibitor Induces Mitotic Arrest and Activates Apoptosis in Cancer Cells. *Sci. Rep.* **2016**, *6* (1), 34653.
(61) Thomas, E.; Gopalakrishnan, V.; Somasagara, R. R.; Choudhary, B.; Raghavan, S. C. Extract of Vernonia Condensata, Inhibits Tumor Progression and Improves Survival of Tumor-Allograft Bearing Mouse. *Sci. Rep.* **2016**, *6* (1), 23255.
(62) Gopalakrishnan, V.; Sharma, S.; Ray, U.; Manjunath, M.; Lakshmanan, D.; Vartak, S. V.; Gopinatha, V. K.; Srivastava, M.; Kempegowda, M.; Choudhary, B.; et al. SCR7, an Inhibitor of NHEJ Can Sensitize Tumor Cells to Ionization Radiation. *Mol. Carcinog.* **2021**, *60* (9), 627−643.
(63) Ray, U.; Gopinatha, V. K.; Sharma, S.; Goyary, L.; Choudhary, B.; Mantelingu, K.; Rangappa, K. S.; Raghavan, S. C. Identification and Characterization of Mercaptopyrimidine-Based Small Molecules as Inhibitors of Nonhomologous DNA End Joining. *FEBS J.* **2023**, *290* (3), 796−820.
(64) Becke, A. D. Density-Functional Exchange-Energy Approximation with Correct Asymptotic Behavior. *Phys. Rev. A* **1988**, *38* (6), 3098−3100.
(65) Bauernschmitt, R.; Häser, M.; Treutler, O.; Ahlrichs, R. Calculation of Excitation Energies within Time-Dependent Density Functional Theory Using Auxiliary Basis Set Expansions. *Chem. Phys. Lett.* **1997**, *264* (6), 573−578.
(66) Trott, O.; Olson, A. J. AutoDock Vina: Improving the Speed and Accuracy of Docking with a New Scoring Function, Efficient Optimization, and Multithreading. *J. Comput. Chem.* **2010**, *31* (2), 455−461.
(67) Wang, E.; Sun, H.; Wang, J.; Wang, Z.; Liu, H.; Zhang, J. Z.; Hou, T. End-Point Binding Free Energy Calculation with MM/PBSA and MM/GBSA: Strategies and Applications in Drug Design. *Chem. Rev.* **2019**, *119* (16), 9478−9508.
(68) Kumari, R.; Kumar, R.; Lynn, A. G_mmpbsa- A GROMACS Tool for High-Throughput MM-PBSA Calculations. *J. Chem. Inf. Model.* **2014**, *54* (7), 1951−1962.

https://doi.org/10.1021/acsomega.3c05816
ACS Omega 2023, 8, 38619−38631